Pergamon

Cement and Concrete Research 30 (2000) 855–863

CEMENT AND CONCRETE RESEARCH

A model for two types of calcium silicate hydrate in the microstructure of Portland cement pastes

Paul D. Tennis[a,1], Hamlin M. Jennings[a,b,*]

[a]*Department of Civil Engineering, Northwestern University, Evanston, IL, 60208 USA*
[b]*Department of Materials Science and Engineering, Northwestern University, Evanston, IL, 60208 USA*

Received 22 February 1999; accepted 6 March 2000

Abstract

A new physical basis for a previously published model for the structure of calcium silicate hydrate (C-S-H) as measured by nitrogen sorption is described. This refined model provides a method of predicting the density, the nitrogen accessible gel porosity, and associated surface area of C-S-H in Portland cement pastes. The basis for the model is that C-S-H forms as one of two types, high- or low-density C-S-H. This provides a promising tool for characterizing the microstructure in a way that can be applied to understanding properties of engineering significance. © 2000 Elsevier Science Ltd. All rights reserved.

Keywords: Modeling; Microstructure; Surface area; Cement paste; Calcium silicate hydrate (C-S-H)

1. Introduction

The microstructures of Portland cement pastes are complex and, in many respects, have not been characterized quantitatively. The main hydration product, calcium silicate hydrate (C-S-H), has a complex internal pore structure with a high specific surface area. Several techniques have been used to measure the surface area, but as indicated in a recent review by Thomas et al. [1], results vary widely. Among the most confusing of the results is BET surface area using nitrogen, partly because the results fluctuate with variables such as internal water:cement ratio. No quantitative explanation has been offered. One problem, addressed in the earlier model [2,3], is that a simple interpretation of higher surface area resulting from a more open C-S-H, and therefore, a pore system more accessible to the nitrogen molecule, is not consistent with the volume of porosity as measured by nitrogen. If this were the case, higher surface areas would be associated with greater volume of measured pores within the C-S-H, the gel pores. The problem is that, in samples of comparable age, after larger capillary porosity is accounted for, the volume of gel porosity measured by nitrogen is smaller in samples with higher surface areas. Put another way, the volume of capillary porosity does not scale with variables such as water:cement ratio. Although the previous model rationalized this problem by creating mathematical boxes, the physical basis for the model remained obscure. This paper describes a new refined model that is based on the possibility of C-S-H forming in the paste with two different densities; a high-density (HD) C-S-H and a low-density (LD) C-S-H.

2. The model

As with the earlier version, the first task is to determine the quantity of C-S-H and other components in the microstructure of cement pastes. The model assumes simple stoichiometric reactions for the hydration of the four dominant compounds in Portland cement, C_3S,[2] C_2S, C_3A, and C_4AF. These have been modified slightly from an earlier version of the model to more

* Corresponding author. Tel.: +1-847-491-4858; fax: +1-847-491-4011.

E-mail address: h-jennings@northwestern.edu (H.M. Jennings).

[1] Present location: Portland Cement Association, Skokie, IL, 60077 USA.

[2] Cement chemists' notation is used throughout; C = CaO; S = SiO_2, A = Al_2O_3; F = Fe_2O_3, $\bar{S}$ = SO_3 H = H_2O. Thus, C_3S = 3CaO·SiO_2. Dashes in the formula for C-S-H emphasize its variable composition.

PII: S0008-8846(00)00257-X

accurately reflect current theories on cement hydration [4] [see Eqs. (1)–(6)]:

$$2C_3S + 10.6H \rightarrow C_{3.4} - S_2 - H_8 + 2.6CH \quad (1)$$

$$2C_2S + 8.6H \rightarrow C_{3.4} - S_2 - H_8 + 0.6CH \quad (2)$$

$$C_3A + 3C\bar{S}H_2 + 26H \rightarrow C_6A\bar{S}_3H_{32} \quad (3)$$

$$2C_3A + C_6A\bar{S}_3H_{32} + 4H \rightarrow 3C_4A\bar{S}H_{12} \quad (4)$$

$$C_3A + CH + 12H \rightarrow C_4AH_{13} \quad (5)$$

$$C_4AF + 2CH + 10H \rightarrow 2C_3(A,F)H_6 \quad (6)$$

The first two equations are the most important as they define the quantity of C-S-H formed. The composition for C-S-H is reasonably well established as being valid in neat Portland cement pastes. Eq. (3) is used for the initial reactions of C_3A in the presence of sulfate to form ettringite. After the initial supply of sulfate is depleted, Eq. (4) is used for additional C_3A hydration to form monosulfoaluminates. Eq. (5) is used for continued hydration of C_3A after all ettringite is consumed. In Eq. (6), the product of the ferrite reaction is a hydrogarnet [5]. Although several other aluminum-bearing compounds are known to form under various conditions [6,7], the set of reactions used here are consistent with current ideas about the nature of early reactions of the interstitial phases and the formation of the major products of long-term hydration. One potential weakness is the assumption that ettringite is completely consumed to form monosulfate even though some ettringite is typically found in well-hydrated pastes and concretes. This may be due to the presence of carbonate-bearing aluminate compounds (for example, hemi- or mono-carboaluminates), but the uncertainties regarding the extent and rate of the reactions, and the potential for a large number of different products make some approximation inevitable. The assumptions chosen for this model are a starting point, and they have a minor effect on the results of the remainder of the model.

Another potential weakness in the model is its dependence on the Bogue calculation for the cement composition. The Bogue calculation is an approximation that has been criticized [8] and improvements have been suggested [9]. In particular, C_4AF is a solid solution with a widely-varying, highly-substituted composition in most cements. Improved quantitative techniques are now available for determining the composition of cements. However, the wide range of historic data used to calibrate the model generally did not provide sufficient characterization to allow alternatives to be used. Thus, these traditional equations are used out of necessity, and as new data become available, the model can be improved with more accurate assumptions.

It should be noted that Eqs. (1)–(6) are balanced assuming all of the hydration products are saturated. For samples that have been dried, such as those used in adsorption experiments to determine surface area, the products of the reactions in Eqs. (1)–(6) are dried to the water contents shown in Table 1, with a corresponding re-balancing of the reactions.

The rates of the reactions assumed for the model are approximations based on Avrami equations of the form [see Eq. (7)]:

$$\alpha_i = 1 - e^{-(a_i(t-b_i)^{c_i})} \quad (7)$$

where α_i is the degree of hydration of compound i at time t (in days). The constants a_i, b_i, and c_i have been determined empirically for a specific Portland cement [10,11] and are used as an approximation for other Portland cements; that is, it is assumed that the compounds react at similar relative rates. These constants are given in Table 2.

Avrami equations are best suited to describing nucleation and growth reactions and therefore, strictly speaking, do not describe the more complex reactions occurring in Portland cements [12,13]. However, they provide a simple kinetic model that allows good fits for kinetics for the first 20–30% reaction and a first approximation for pastes

Table 1
Key parameters used in the model

Compound	Nominal formula	Density (kg/m^3)	Molecular weight (kg/mol)	Molar volume (10^{-5} m^3/mol)
Alite	C_3S	3150	0.228	7.24
Belite	C_2S	3280	0.172	5.24
Aluminate	C_3A	3030	0.270	8.92
Ferrite	C_4AF	3730	0.486	13.03
Water	H_2O	998	0.018	1.80
Gypsum	$C\bar{S}H_2$	2320	0.172	7.41
Calcium hydroxide	CH	2240	0.074	3.31
Hydrogarnet	$C_3(A,F)H_6$	2670	0.407	15.27
AFm, saturated	$C_4A\bar{S}H_{12}$	1990	0.623	34.6
AFm, dried	$C_4A\bar{S}H_8$	2400	0.551	22.9
AFt, saturated	$C_6A\bar{S}_3H_{32}$	1750	1.255	71.7
AFt, dried	$C_6A\bar{S}_3H_7$	2380	0.805	33.8
Calcium aluminate hydrate	C_4AH_{13}	2050	0.560	27.4
LD C-S-H, dried	$C_{3.4}S_2H_3$	1440	0.365	25.2
HD C-S-H, dried	$C_{3.4}S_2H_3$	1750	0.365	21.1

Table 2
Constants used in the Avrami equations [11]

Compound *i*	a	b	c
C_3S	0.25	0.90	0.70
C_2S	0.46	0	0.12
C_3A	0.28	0.90	0.77
C_4AF	0.26	0.90	0.55

hydrated more than 1 day. Better models to describe Portland cement hydration exist (e.g., Refs. [14,15]), and it is anticipated that better kinetic models will replace this one in the future. The main advantage of this approach is the ability to apply separate rates of reaction to different minerals in Portland cement. In practice, a closer approximation is obtained by iterating through time until a weighted average for the degrees of reaction of the individual compounds matches a specific degree of hydration chosen. Fig. 1 shows the percentage of reaction of the individual compounds and an average[3] Type I Portland cement [16] as a function of time using Eq. (7) with the constants provided in Table 2.

Given the composition of the cement and the water:-cement ratio, the governing chemical and kinetic equations provide a means of computing the quantity of the various phases present in the microstructure at any given time. The percentage of capillary porosity, V_{cp}, is calculated as follows [see Eq. (8)]:

$$V_{cp} = V_w - \sum_i (V_p - V_r) \tag{8}$$

where V_w is the initial volume percent of water, V_p is the volume percent of hydration product, V_r is the volume percent of reactant, and the summation is over all reactions, *i*. The volume of gel porosity is included in the volume of C-S-H. As an example, the relative volumes of each of the phases in a typical Portland cement paste are plotted as a function of the degree of hydration of the paste in Fig. 2.

2.1. C-S-H

As stated above, surface area as measured by nitrogen can be modeled [2] by dividing C-S-H into two types: one that is "seen" by nitrogen and one that is not. The present model proposes a physical basis for the two regions of C-S-H based on their densities: HD C-S-H and LD C-S-H. As shown in Fig. 3, the proposed HD and LD C-S-H can explain how higher surface areas (measured by nitrogen) are associated with smaller volume of gel pores accessible to nitrogen, and vice versa. It should be noted that this has nothing to do with the variations in surface areas resulting from variables such as drying technique.

There is other evidence for different types of C-S-H. They may correspond to the C-S-H portions of phenograins and groundmass regions observed by scanning electron microscopy [17], inner and outer product [18,19], or middle and late product [20]. The HD C-S-H is relatively stable under the high vacuum required for electron microscopy, while the LD C-S-H is considerably less stable. These microscopic observations support the concept of two different forms of C-S-H in Portland cement pastes. This concept of two types of C-S-H is also supported by recent observations using neutron scattering [1].

In this model, the distribution of C-S-H into each type is determined by assuming that the LD C-S-H is the only component of the microstructure that contributes appreciably to the surface area as measured by nitrogen. Each type of C-S-H contains a specific amount of total gel porosity: none of the pores in HD C-S-H are accessible to nitrogen, while only some of the pores in LD C-S-H are accessible to nitrogen. Data [21] for surface area measured by nitrogen adsorption on D-dried pastes are shown in Table 3. These data are used to calibrate the model by defining M_r, the ratio of the mass of LD C-S-H to the total mass of C-S-H [see Eq. (9)]:

$$M_r = \frac{S_{N_2} M_D}{S_{LD} M_t} \tag{9}$$

where S_{N2} is the specific surface area of the dried paste

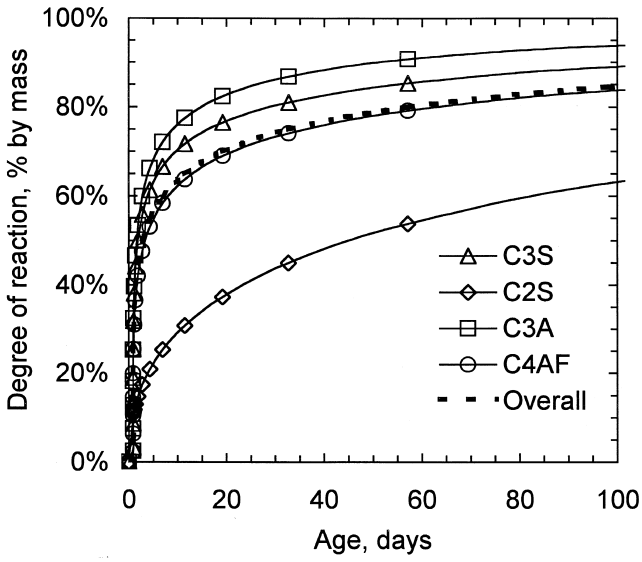

Fig. 1. Each of the principal compounds is assumed to hydrate independently as shown. A degree of reaction for the cement is computed using a weighted average. The curve labeled "weighted average" in this plot has a composition of 55% C_3S, 18% C_2S, 10% C_3A, and 8% C_4AF, an average Type I cement composition [16].

[3] The composition of the Portland cement chosen for the examples in Figs. 1 and 2 is based on an extensive survey of Portland cements produced in North America in 1994 [16] and is an average for Type I cements.

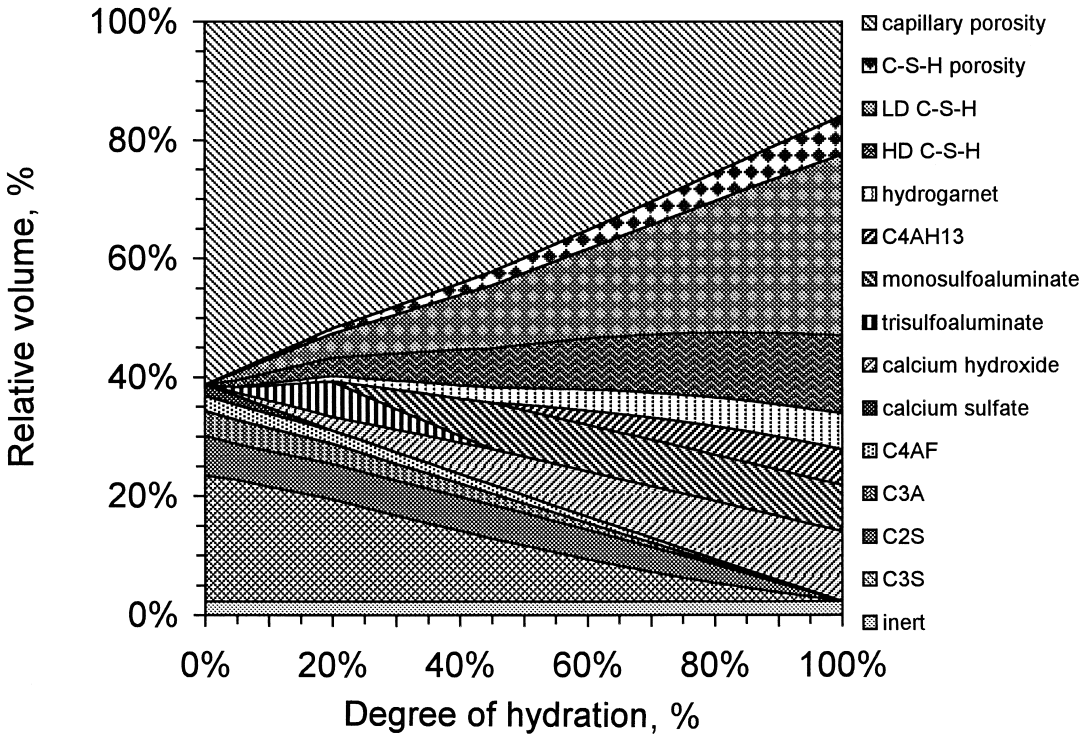

Fig. 2. Relative volume of each of the phases (as predicted by the model) as a function of the degree of hydration. The example is for a paste with water:cement ratio of 0.50, and 55% C_3S, 18% C_2S, 10% C_3A, and 8% C_4AF, an average Type I cement composition [16].

(determined from nitrogen sorption isotherms), M_D is the mass of dried paste, S_{LD} is the surface area per gram of D-dried LD C-S-H (which is not independently measurable), and M_t is the total mass of C-S-H. Using multiple linear regression, an equation for M_r is obtained that is applied to other data [see Eq. (10)]:

$$M_r = 3.017(w:c)\alpha - 1.347\alpha + 0.538 \quad (10)$$

where w:c is the water:cement ratio and α is the degree of hydration. The mass ratio calculated via Eq. (10) is shown in Fig. 4. All coefficients in Eq. (10) are statistically significant at the 95% confidence level.

The volume percentage of HD C-S-H is given by Eq. (11):

$$V_{HD} = \frac{M_t - (M_r M_t)}{\rho_{HD}} \quad (11)$$

and the volume percentage of LD C-S-H by Eq. (12):

$$V_{LD} = \frac{M_r M_t}{\rho_{LD}} \quad (12)$$

where V_x is the volume of x, ρ_x is the density of x, and M_t is the total mass of C-S-H. Note that this term assumes that the C-S-H is dried (i.e., no water is included in the pores of C-S-H, but the empty pores are included).

As will be seen by the densities computed by optimizing this model, HD C-S-H must have some porosity and LD C-S-H has more porosity. The additional volume of pores in LD C-S-H is shown in Eq. (13):

$$V_P = V_{LD} - \frac{M_r M_t}{\rho_{HD}} \quad (13)$$

where V_P is the volume of additional porosity in the LD

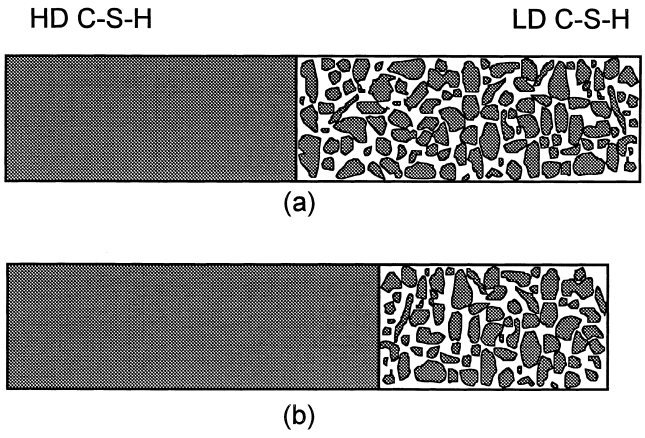

Fig. 3. A schematic diagram of the two-density model of C-S-H as seen by nitrogen. The regions on the left represent HD C-S-H and regions on the right represent LD C-S-H. Particles of LD C-S-H are accessible to nitrogen for surface area and porosity measurements via nitrogen. No surface area or porosity is measured using nitrogen in HD C-S-H. Boxes represent equal degrees of hydration for: (a) a higher water:cement ratio (0.50) and (b) a lower water:cement ratio (0.35).

Table 3
Specific surface areas of portland cement pastes, as measured by nitrogen sorption [21]

Water: cement ratio	Age (days)	Specific surface area (m^2/g ignited paste)		D-dried mass[a] (g per g paste)	Ignited mass[b] (g per g paste)	Specific surface area (m^2/g D-dried paste)	
0.251	1	15.5	15.7	0.858	0.799	14.4	14.6
0.251	7	13.9	14.0	0.889	0.799	12.5	12.6
0.251	28	15.1	13.4	0.903	0.799	13.4	11.9
0.251	180	13.2	13.2	0.921	0.799	11.5	11.5
0.333	1	18.5	18.8	0.796	0.750	17.4	17.7
0.333	7	24.7	23.9	0.838	0.750	22.1	21.4
0.333	28	31.7	33.7	0.866	0.750	27.4	29.2
0.333	180	42.3	35.3	0.884	0.750	35.9	29.9
0.442	1	18.2	18.4	0.738	0.693	17.1	17.3
0.442	7	32.3	34.9	0.772	0.693	29.0	31.4
0.442	28	47.8	49.9	0.802	0.693	41.3	43.1
0.442	180	70.3	71.1	0.830	0.693	58.7	59.4
0.501	1	20.7	20.6	0.707	0.666	19.5	19.4
0.501	7	31.4	34.1	0.735	0.666	28.5	30.9
0.501	28	52.5	53.3	0.757	0.666	46.2	46.9
0.501	180	81.6	84.4	0.794	0.666	68.5	70.9

[a] Determined using the model.
[b] Assumes ignited mass equal to initial cement mass.

C-S-H. This is the volume of porosity in the C-S-H that is accessible to nitrogen.

Thus, the values remaining to be determined are S_{LD}, ρ_{HD}, and ρ_{LD}. These are the parameters that must be fit by optimizing the model.

3. Optimization

An iterative process has been used to optimize the values of S_{LD}, ρ_{HD}, and ρ_{LD} based on the fit between measured values for surface area and porosity (both measured by nitrogen sorption), and capillary porosity and the values for those quantities predicted by the model. The values for capillary porosity have been determined using solvent replacement [2], sorption of large molecules [23], mercury porosimetry [28], and estimation from evaporable water contents [29]. These techniques measure different properties; however, assumptions made in each of those studies (for example, using the volume of mercury intruded above a pore diameter of 20 nm) yield estimates of capillary porosity consistent with the values predicted by the model. The criterion for measuring the goodness-of-fit is the fit coefficient, f, as defined by Popovics [22]. This parameter is similar to the correlation coefficient, r, in linear regression, but it is related to the dispersion about the line $y = x$, rather

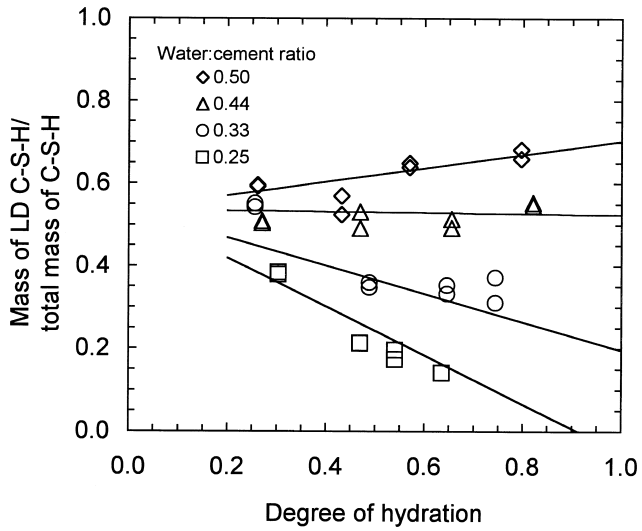

Fig. 4. M_r is the mass ratio of LD C-S-H to total C-S-H. The division of C-S-H into low- and high-density regions is a function of water:cement ratio and degree of hydration and is based on regression analyses of Hunt's [21] data. Lines are model estimates, and points are Hunt's data. $r^2 = 0.932$.

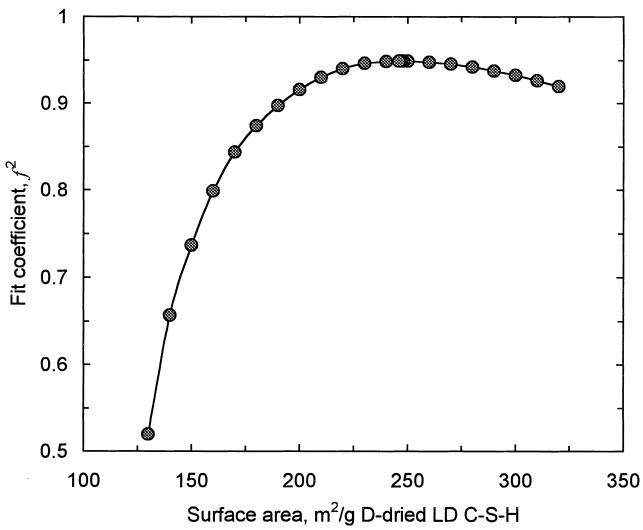

Fig. 5. To optimize the model, the specific surface area of LD C-S-H is varied. Values above 200 m^2/g provide high degrees of fit between measured and predicted values; a maximum fit is obtained at 247 m^2/g dried LD C-S-H.

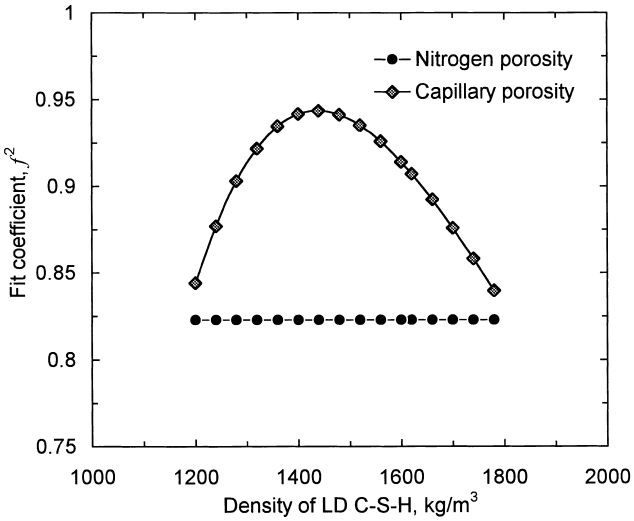

Fig. 6. The goodness-of-fit between the model's predictions and measured values of capillary porosity is influenced by the value of the density chosen for the LD C-S-H. The fit for porosity accessible to nitrogen shows almost no variation with density. The optimum value for LD C-S-H is 1440 kg/m^3.

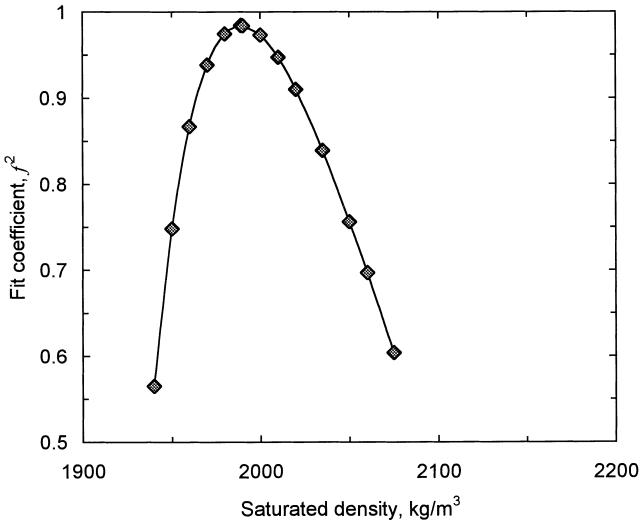

Fig. 8. The goodness-of-fit between the model's predictions and measured values of chemical shrinkage is heavily influenced by the value of the density chosen for saturated C-S-H. The optimum value for saturated C-S-H density is 1990 kg/m^3.

than a best fit line. The value of f can range between 0 and 1, but f^2 can never be larger than r^2. The higher values of f^2 in Figs. 5–7 indicate better fit between the measured values and values predicted by the model.

Fig. 5 shows the fit coefficient obtained between surface areas determined using nitrogen sorption from several laboratories [21,23–25] and values predicted by the model using different values of S_{LD}. The curve rises to a plateau at about $f^2 = 0.948$ with a maximum at 247 m^2/g D-dried LD C-S-H. Once a certain value of S_{LD} is reached, no additional improvement in the model is gained by increasing this specific surface area.

As shown in Fig. 6, the optimum fit between measured values for capillary porosity [23,25–29] and values predicted by the model varies strongly with ρ_{LD}. The value chosen for ρ_{LD} has no impact on the fit for porosity accessible to nitrogen. Increasing the density for LD C-S-H leads to larger values of capillary porosity and smaller values of gel porosity accessible to nitrogen; these changes counteract each other, and the total porosity accessible to nitrogen is unchanged. A reverse trend is observed in Fig. 7; the value of the fit coefficient for porosity accessible to

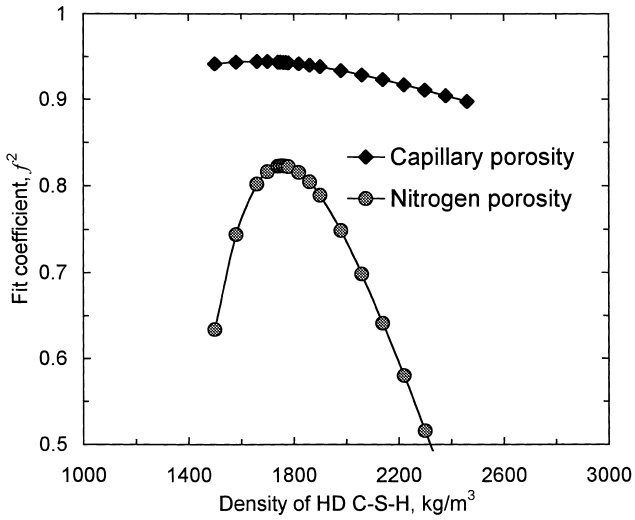

Fig. 7. The goodness-of-fit between the model's predictions and measured values of porosity accessible to nitrogen is influenced by the value of density chosen for the HD C-S-H. The fit for capillary porosity shows no variation with the density. The optimum value for HD C-S-H is 1750 kg/m^3.

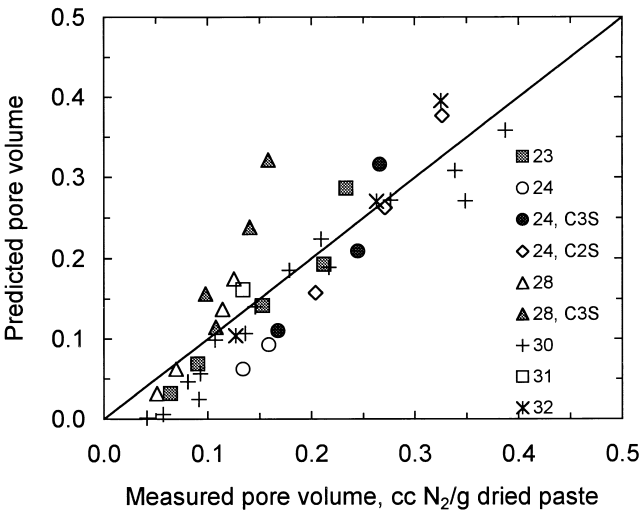

Fig. 9. The predicted and measured values of the volume of pores (as measured by nitrogen). The line represents a perfect prediction. The fit coefficient (f^2) between the points and the line is 0.823. Sources of data are provided in the legend [23,24,28,30–32].

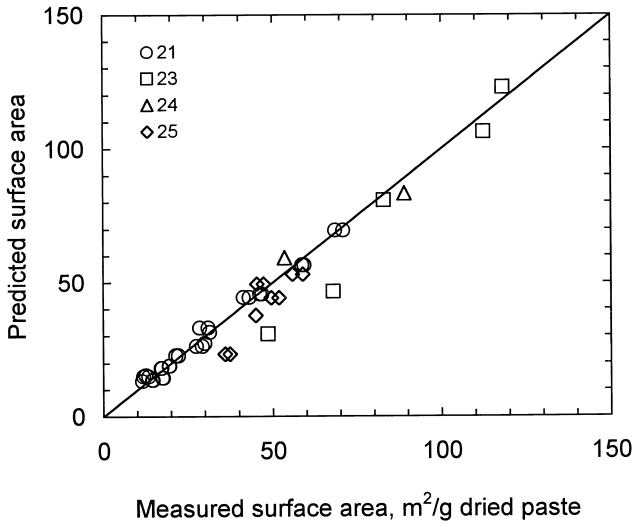

Fig. 10. The predicted and measured values of surface areas (as measured by nitrogen). The line represents a perfect prediction. The fit coefficient (f^2) between the points and the line is 0.947. Sources of data are provided in the legend [21,23–25].

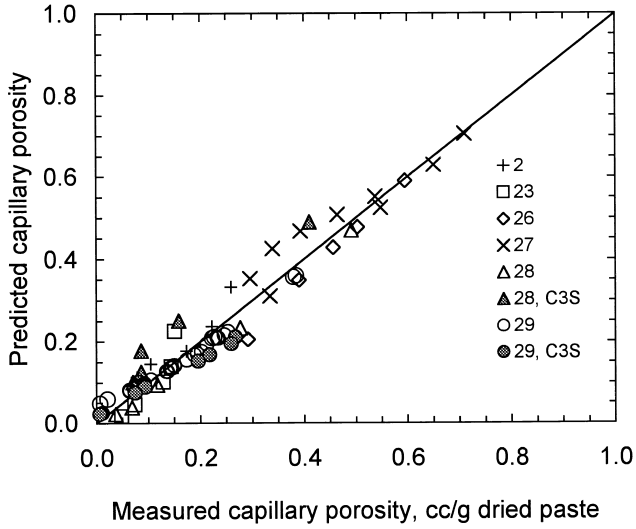

Fig. 11. The predicted and measured values of capillary porosity (as measured by solvent exchange, adsorption, mercury porosimetry, and evaporable water content). The line represents a perfect prediction. The fit coefficient (f^2) between the points and the line is 0.944. Sources of data are provided in the legend [23,26–29].

nitrogen shows a distinct maximum when plotted against ρ_{HD}, whereas the value of ρ_{HD} has little impact on the fit for capillary porosity. Increasing the value for ρ_{HD} increases values predicted for both capillary porosity and porosity accessible to nitrogen. In Fig. 6, the maximum of $f^2 = 0.944$ is at a value for ρ_{LD} of 1440 kg/m^3, while in Fig. 7, the maximum value of the fit coefficient for porosity accessible to nitrogen is $f^2 = 0.822$, which is at a value of $\rho_{HD} = 1750$ kg/m^3.

Chemical shrinkage is estimated by calculating the changes in volume that occur for each of the reactions in Eqs. (1)–(6). In this case, the saturated densities in Table 1 are used because measurements of chemical shrinkage are performed on samples that have never been dried. Measured values [33] of chemical shrinkage for OPC pastes cured at 20°C were used to calibrate the average value of the density of C-S-H in the saturated state. Fig. 8 shows the results of changes to saturated density on the fit coefficient for the calibration data. The maximum fit occurs at $\rho_{sat} = 1990$ kg/m^3, with a fit coefficient, $f^2 = 0.984$. Powers [34] determined a value of 2050 kg/m^3, and Taylor [8] reports a value of 1900 kg/m^3.

4. Results and discussion

Figs. 9–11 show plots of predicted and measured values for surface area, capillary porosity, and porosity accessible to nitrogen, respectively, using the optimum values of $\rho_{LD} = 1440$ kg/m^3, $\rho_{HD} = 1750$ kg/m^3, and $S_{LD} = 247$ m^2/g D-dried LD C-S-H. Data for specific surface area and volume of porosity from a wide range of sources, both reported in the literature and measured in our laboratory, have been compared to similar values predicted by the model. The values of f^2 are 0.823, 0.947, and 0.949, respectively, for predicted values and measured values of surface area, capillary porosity, and porosity accessible to nitrogen. The relatively high fit coefficients support the hypothesis of two types of C-S-H with different densities.

Fig. 12 provides observed and measured values of chemical shrinkage using $\rho_{sat} = 1990$ kg/m^3. The value of the fit coefficient is 0.984. The slight deviations above 4 or 5 cm^3/100 g cement are possibly due to the closing off of porosity due to hydration. Thus, the experimental values may be slightly low, which cannot be accounted for by the model.

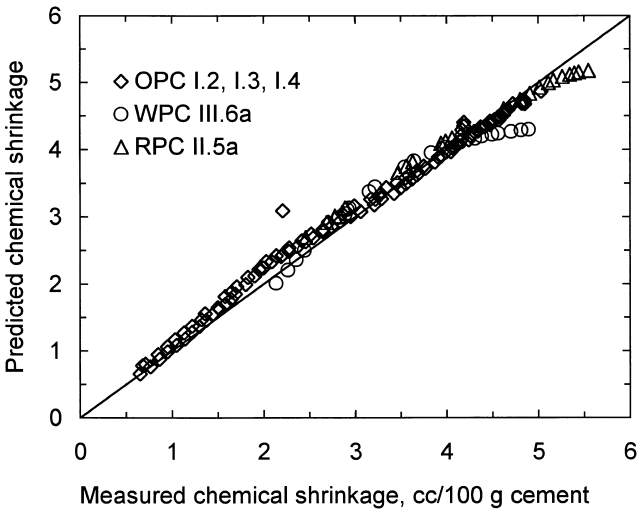

Fig. 12. The predicted and measured [33] values for chemical shrinkage. The fit coefficient (f^2) between the points and the line is 0.982.

If the "true" density of C-S-H solids, exclusive of pores, is taken as 2700 kg/m^3 [8], then the volume of pores not accessible to nitrogen can be calculated: HD C-S-H is 35% by volume, and LD C-S-H is 47% by volume. If this porosity is filled with water (1000 kg/m^3), then HD C-S-H has a density of 2100 kg/m^3 when saturated and LD C-S-H has a saturated density of 1910 kg/m^3. For HD C-S-H:LD C-S-H ratios associated with a 75% hydrated paste at a water:cement ratio of 0.50, the saturated density of C-S-H is 1980 kg/m^3. This is nearly the same value determined by optimizing the model for predictions of chemical shrinkage. Data independently measured for both chemical shrinkage and specific surface area is therefore consistent with the model incorporating two types of C-S-H.

If a value of 2500 kg/m^3 is used for the density exclusive of pores [8], perhaps a more realistic value based on metajennite or 1.1 nm tobermorite, then HD C-S-H contains 30% porosity and the LD C-S-H contains 42%. The saturated densities are 2050 and 1860 kg/m^3, respectively. This leads to a lower value for the saturated density for the case noted above (water:cement ratio = 0.50, 75% hydrated) of 1920 kg/m^3, a value lower than the 1990 kg/m^3 determined by optimizing for chemical shrinkage, but within 5%.

It is worth noting that attempts to optimize this model using a pore system in the LD C-S-H that is completely accessible to nitrogen does not provide a good fit between the measured values for total porosity (pores accessible to nitrogen) and model estimates. The best fit obtainable is $f^2 = 0.692$. This is because the volume of porosity is substantially overpredicted at higher water:cement ratios (higher total porosity) and significantly underpredicted at lower water:cement ratios.

By studying the changes required to make the model fit data for cementitious systems other than neat pastes, such as the inclusion of chemical or mineral admixtures, curing at different temperatures, or curing under varying relative humidity conditions, further information about the structure of C-S-H can be obtained.

This microstructural model is notable in that it includes a physical basis for two types of C-S-H in Portland cement pastes, each with its own density. By providing a means for determining quantitative estimates of the amounts of each phase in the microstructure, it is believed that stronger correlation between microstructure and physical properties such as creep and shrinkage and transport properties may be developed.

5. Conclusions

A revised model of the microstructure of Portland cement paste has been presented that quantitatively predicts the volumes of the various phases. The pore structure, including capillary porosity, porosity accessible to nitrogen, and specific surface area are all accurately predicted. In addition, values for chemical shrinkage of neat pastes predicted by the model also correspond well to physical measurements. A key element of this model is a division of C-S-H into two types, each with a specific density.

Acknowledgments

The support of the Department of Energy, award number DE-FG02-91ER45460, is gratefully acknowledged.

References

[1] J.J. Thomas, H.M. Jennings, A.J. Allen, The surface area of cement paste as measured by neutron scattering: evidence for two C-S-H morphologies, Cem Concr Res 28 (6) (1998) 897–905.
[2] H.M. Jennings, P.D. Tennis, Model for the developing microstructure in Portland cement pastes, J Am Ceram Soc 77 (12) (1994) 3161–3172.
[3] H.M. Jennings, P.D. Tennis, Correction: model for the developing microstructure in Portland cement pastes, J Am Ceram Soc 78 (9) (1995) 2575.
[4] RILEM Committee 68-MMH, Task Group 3, The hydration of tricalcium aluminate and tetracalcium aluminoferrite in the presence of calcium sulfate, Mater Struct 19 (10) (1986) 137–147.
[5] H.F.W. Taylor, personal communication, June 27, 1995.
[6] W.A. Klemm, Ettringite and Oxyanion-Substituted Ettringites—Their Characterization, and Applications in the Fixation of Heavy Metals: A Synthesis of the Literature, Portland Cement Assn. RD116, Skokie, IL, 1998.
[7] R.L. Day, The Effect of Secondary Ettringite Formation on the Durability of Concrete: A Literature Analysis, Portland Cement Assn. RD108, Skokie, IL, 1992.
[8] H.F.W. Taylor, Cement Chemistry, 2nd edn, Thomas Telford, London, 1997.
[9] H.F.W. Taylor, Modification of the Bogue calculation, Adv Cem Res 2 (6) (1989) 73–77.
[10] J.A. Dalziel, W.A. Gutteridge, The influence of pulverized-fuel ash upon the hydration characteristics and certain physical properties of a Portland cement paste, Cem and Concr Assoc, Tech Rep Slough, England, 560.
[11] H.F.W. Taylor, A method for predicting alkali ion concentration in cement pore solutions, Adv Cem Res 1 (1) (1987) 5–17.
[12] E.M. Gartner, J.M. Gaidis, Hydration mechanisms I, in: J.P. Skalny (Ed.), Materials Science of Concrete I, The American Ceramic Society, Cincinnati, OH, 1989, pp. 95–125.
[13] P.W. Brown, J.M. Pommersheim, G. Frohnsdorff, Kinetic modeling of hydration processes, in: J.F. Young (Ed.), Cements Research Progress 1983, The American Ceramic Society, Cincinnati, OH, 1984, pp. 245–260.
[14] T. Knudsen, The dispersion model for hydration of Portland cement, Cem Concr Res 14 (5) (1984) 622–630.
[15] A. Saglik, A Mathematical Model for the Kinetics of Portland Cement Hydration, MS Thesis, Northwestern University, Evanston, IL, 1992.
[16] R.F. Gebhardt, Survey of North American Portland cements: 1994, Cem Concr Agg 17 (2) (1995) 145–189.
[17] S. Diamond, D. Bonen, Microstructure of hardened cement paste—a new interpretation, J Am Ceram Soc 76 (12) (1993) 2993–2999.
[18] S. Chatterji, J.W. Jeffrey, Studies of early stages of paste hydration of cement compounds I, J Am Ceram Soc 45 (11) (1962) 536–543.
[19] F.V. Lawrence Jr., J.F. Young, Studies on the hydration of tricalcium silicate pastes: I. Scanning electron microscopic examination of microstructural features, Cem Concr Res 3 (2) (1973) 149–161.

[20] H.M. Jennings, B.J. Dalgleish, P.L. Pratt, Morphological development of hydrating tricalcium silicate as examined by electron microscopy, J Am Ceram Soc 64 (10) (1981) 567–572.
[21] C.M. Hunt, Nitrogen sorption measurements and surface areas of hardened cement pastes, Proc of a Symp on the Structure of Portland Cement Paste and Concrete, Highway Res. Board Sp. Rep. 90, National Academy of Engineering, Washington, DC, 1966, pp. 112–122.
[22] S. Popovics, A method for evaluating how well observed data fit the line $Y = X$, Mater Res Stand 7 (5) (1967) 195–202.
[23] R.Sh. Mikhail, S.A. Selim, Adsorption of organic vapors in relation to the pore structure of hardened Portland cement paste, Proc of Symp on the Structure of Portland Cement Paste and Concrete, Highway Res. Board Sp. Rep. 90, National Academy of Engineering, Washington, DC, 1966, pp. 123–132.
[24] J. Hagymassy Jr., I. Odler, M. Yudenfreund, J. Skalny, S. Brunauer, Pore structure analysis by water vapor adsorption: III. Analysis of hydrated calcium silicates and Portland cements, J Colloid Interface Sci 38 (1) (1972) 20–34.
[25] M. Garci, unpublished data, 1996.
[26] L.J. Parrott, R.G. Patel, D.C. Killoh, H.M. Jennings, Effect of age on diffusion in hydrated alite cement, J Am Ceram Soc 67 (4) (1984) 233–237.
[27] L.J. Parrott, Measurement and modeling of porosity in drying cement paste, in: L.J. Struble, P.W. Brown (Eds.), Microstructural Development During Hydration of Cement, Mater Res Soc Symp Proc, vol. 85, Materials Research Society, Pittsburgh, PA, 1987, pp. 91–104.
[28] I. Odler, H. Köster, Investigations on the structure of fully hydrated Portland cement and tricalcium silicate pastes: II. Total porosity and pore size distribution, Cem Concr Res 16 (6) (1986) 893–901.
[29] R.A. Helmuth, D.H. Turk, Elastic moduli of hardened Portland cement pastes: effect of porosity, Proc of a Symp on the Structure of Portland Cement Paste and Concrete, Highway Res. Board Sp. Rep. 90, National Academy of Engineering, Washington, DC, 1966, pp. 135–144.
[30] H. Uchikawa, S. Uchida, S. Hanehara, Measuring method of pore structure in hardened cement paste, mortar and concrete, Cemento 88 (2) (1991) 67–90.
[31] M. Daimon, S.A. Abo-El-Enein, G. Hosaka, S. Goto, R. Kondo, Pore structure of calcium silicate hydrate in hydrated tricalcium silicate, J Am Ceram Soc 60 (3–4) (1977) 110–114.
[32] W. Hansen, J. Almudaiheem, Pore structure of hydrated Portland cement measured by nitrogen sorption and mercury intrusion porosimetry, in: L.J. Struble, P.W. Brown (Eds.), Microstructural Development During Hydration of Cement, Mater Res Soc Symp Proc, vol. 85, Materials Research Society, Pittsburgh, PA, 1987, pp. 105–114.
[33] M. Geiker, Studies of Portland Cement Hydration by Measurements of Chemical Shrinkage and a Systematic Evaluation of Hydration Curves by Means of the Dispersion Model, PhD Thesis, Institute of Mineral Industry, Technical University of Denmark, 1983.
[34] T.C. Powers, Adsorption of water by Portland cement paste during the hardening process, Ind Eng Chem 27 (7) (1935) 790–794.